Nanotechnology **22** (2011) 315101 (5pp) doi:10.1088/0957-4484/22/31/315101

Modeling the conductance and DNA blockade of solid-state nanopores

Stefan W Kowalczyk[1], **Alexander Y Grosberg**[2], **Yitzhak Rabin**[3,4,5] **and Cees Dekker**[1]

[1] Kavli Institute of Nanoscience, Delft University of Technology, Lorentzweg 1, 2628 CJ Delft, The Netherlands
[2] Department of Physics and Center for Soft Matter Research, New York University, 4 Washington Place, New York, NY 10003, USA
[3] Department of Physics and Institute for Nanotechnology and Advanced Materials, Bar Ilan University, Ramat Gan 52900, Israel
[4] Department of Biomedical Engineering, Northwestern University Evanston, IL 60208, USA
[5] James Franck Institute, University of Chicago, Chicago, IL 60637, USA

E-mail: c.dekker@tudelft.nl

Received 14 March 2011, in final form 14 June 2011
Published 6 July 2011
Online at stacks.iop.org/Nano/22/315101

Abstract
We present measurements and theoretical modeling of the ionic conductance G of solid-state nanopores with 5–100 nm diameters, with and without DNA inserted into the pore. First, we show that it is essential to include access resistance to describe the conductance, in particular for larger pore diameters. We then present an exact solution for G of an hourglass-shaped pore, which agrees very well with our measurements without any adjustable parameters, and which is an improvement over the cylindrical approximation. Subsequently we discuss the conductance blockade ΔG due to the insertion of a DNA molecule into the pore, which we study experimentally as a function of pore diameter. We find that ΔG decreases with pore diameter, contrary to the predictions of earlier models that forecasted a constant ΔG. We compare three models for ΔG, all of which provide good agreement with our experimental data.

S Online supplementary data available from stacks.iop.org/Nano/22/315101/mmedia

(Some figures in this article are in colour only in the electronic version)

Solid-state nanopores, nanometer-sized holes in a thin synthetic membrane, are a versatile tool for the detection and manipulation of charged biomolecules [1, 2]. An external electric field drives a biomolecule through the nanopore, producing a characteristic transient change in the trans-pore ionic current. This approach can be used for sensitive single-molecule biosensing platforms, and much current research is directed toward nanopore sequencing of DNA.

An understanding of the conductance of a nanopore is the basis for any nanopore experiment. To date, however, models for conductance through nanopores have been rather oversimplified [3]. In most previous studies of DNA translocation through nanopores, with a few exceptions [4, 5], it was assumed that (a) the potential drop occurs predominantly across the pore and (b) the pore has a cylindrical shape. However, in many cases, particularly when the pore is relatively wide and not very long, the resistance of the medium outside the pore, called the access resistance, and the corresponding potential drop are significant [6–9]. Furthermore, it has been experimentally measured that solid-state nanopores are hourglass-shaped rather than cylindrical [10–14]. Simple models that do not include these factors predict incorrect open pore conductance values G (especially for wide pores with pore diameters larger than the membrane thickness), as well as constant conductance blockade values ΔG independent of pore diameter, in contradiction with experimental data.

We therefore develop a more realistic parameter-free model for the ionic conductance of an hourglass-shaped (hyperboloid) nanopore that captures both the pore-dominated and access-dominated regimes of resistance. Comparison of theoretical predictions and experimental data shows an excellent match between the two. Furthermore, we address the question: how does the ionic conductance change upon

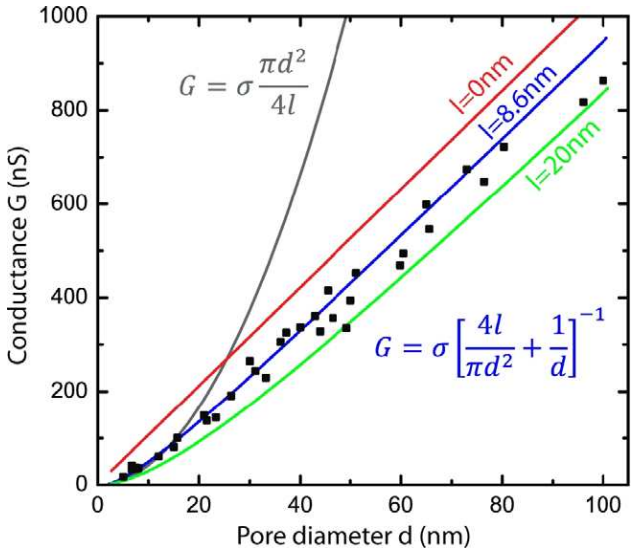

Figure 1. Experimental data for conductance versus pore diameter of pores drilled into a 20 nm thin silicon nitride (SiN) membrane. The solid lines are fits to equation (1) (gray line, $l = 20$ nm) and equation (2) (red, $l = 0$; blue, $l = 8.6$ nm; green, $l = 20$ nm).

insertion of a DNA molecule into the pore? To answer this, we measure how ΔG depends on pore size, and compare the results with simple geometrical models of either a cylindrical or an hourglass-shaped pore.

We measure the conductance versus pore diameter of pores drilled into a 20 nm thin silicon nitride (SiN) membrane. Detailed information about the experiments is presented in section 1. Briefly, a membrane with a nanopore is mounted in a microfluidic flow cell and sealed to liquid compartments on both sides of the sample. Measurements are performed in 1 M KCl salt solution containing 10 mM Tris-HCl and 1 mM EDTA at pH 8.0 at room temperature. Voltages between −0.2 and +0.2 V are applied across the pore and ionic currents are recorded. Fully linear current–voltage curves are obtained in this range of voltages. We measured the conductance for a large number of nanopores with diameters in the range of 5–100 nm, see figure 1. We observe a slightly nonlinearly rising conductance with increasing pore diameter.

We first address the question: how can the conductance ($G = I/V$, the reciprocal of the resistance) of these pores be modeled? Note that we limit ourselves to geometry-based models for the conductance because we consider the high-salt limit where one can neglect the effect of surface charges on the membrane. We first consider the simple expression for a cylindrical pore that is frequently used in the nanopore literature [3]:

$$G = \sigma \frac{\pi d^2}{4l}. \tag{1}$$

Here the bulk conductivity σ (10.5 S m^{-1} at 23 °C [15]) is the reciprocal of the bulk resistivity ρ, d is the diameter of the circular pore, and l is the thickness of the membrane. Note that the only role of the membrane is the obstruction of space available for the current; no other physical effects are considered. A fit of this equation to the data (gray line in figure 1(a)) shows that while in the narrow pore regime ($d \leqslant 15$ nm) the data are well described by the above equation, the model fits the data very poorly for larger pore diameters. The reason for the discrepancy is that the access resistance, which is neglected in equation (1), becomes the dominant contribution at larger pore diameters.

The concept of access resistance stems from the following fact known in general physics (see, for example, [16]): if we consider the electrical resistance of a medium between two spherical electrodes submerged in that medium, then this resistance—quite surprisingly at first glance—does not depend on the distance between the electrodes, but only on their sizes. This happens because the resistance is dominated by the narrow region where the electric current approaches the electrode. More specifically, the resistance between two spherical electrodes in an infinite medium equals $4\rho/\pi d$, where d is the diameter of the electrode. Based on this idea, Hille [6, 7] argued that the access resistance of a pore should also depend only on the pore dimension, and not on any macroscopic dimensions. Specifically, he estimated the access resistance by considering a semi-spherical cupola above the pore entrance as an effective electrode, leading to $R_{\text{access}} = \rho/\pi d$. The coefficient is explained by the fact that, first, we have only one electrode of size d, while the other one is macroscopic and its access resistance is negligible; and, second, we have only half a sphere on one side of the pore. Later on, Hall [8] realized that a semi-spherical cupola is not a reasonable representation of the actual electrode. He considered instead a planar disc at the pore entrance, and obtained $R_{\text{access}} = \rho/2d$. In this paper we will adopt this equation for the access resistance.

As was noted before [9], one can subsequently write the total resistance of a nanopore as

$$R = R_{\text{channel}} + 2R_{\text{access}}. \tag{2}$$

Hence, using the equation from Hall, we obtain the following equation for the conduction:

$$G = \sigma \left[\frac{4l}{\pi d^2} + \frac{1}{d}\right]^{-1}. \tag{3}$$

A least-square fit shows that this equation gives an excellent fit to the data ($\chi^2_{\text{red}} = 1.44$) for a membrane thickness of $l = 8.6$ nm (blue line in figure 1). The fact that this value of l is lower than the given 20 nm membrane thickness is a consequence of the non-cylindrical, hourglass shape of the pore that is due to the e-beam drilling process [10–14]. As a result, the pore diameter is larger at the entrance and exit than at the middle of the membrane, and the effective pore length is lower than the membrane thickness.

The actual shape of a nanopore, as obtained from electron microscopy tomographs [10–14], is typically much closer to an hourglass shape than to a cylindrical shape. We therefore now consider hourglass-shaped pores. Unlike a cylindrical pore, an hourglass-shaped pore is characterized by three lengths: in addition to l (membrane thickness) and d (narrowest diameter), there is also the widest diameter (at the membrane surface) D

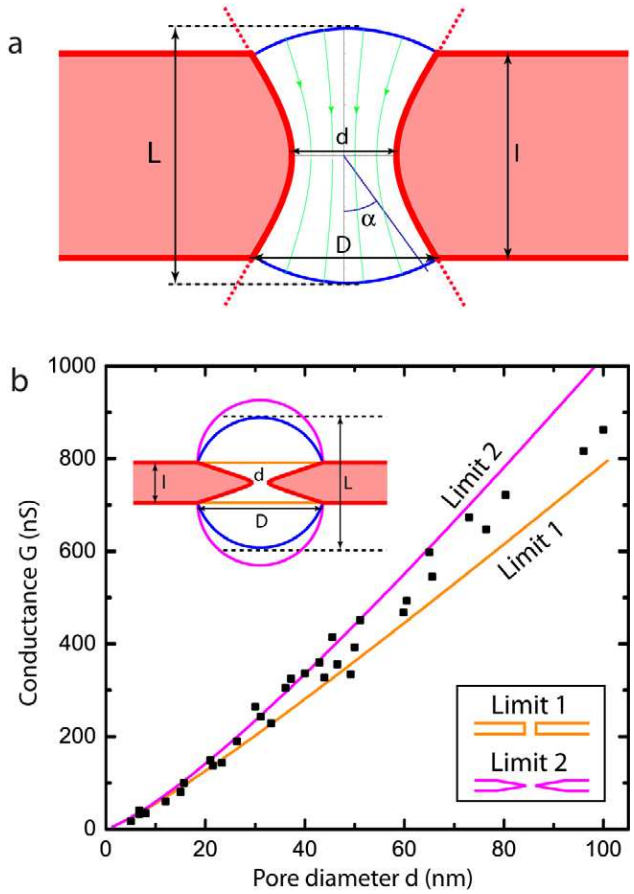

Figure 2. (a) Cross section of an hourglass-shaped nanopore for which the solution in the closed form is obtained. The thick red lines show the surfaces of the SiN dielectric membrane. The thick blue lines indicate equipotentials. The thin green lines are current lines. The angle α, lengths L, l, and diameters d, D are shown. In this image, $d = 1$, $L = 5$, $\alpha = \pi/5$. (b) Experimental data of figure 1 with solid lines that are the predictions from the exact model (equation (7)) with an upper and lower limit for the access resistance. Note that the model fits the data quite well with no free parameters. As expected, the experimental values lie within the two limits. The inset at the bottom right shows pore shapes with $D = d$ (orange) and with $D \gg d$ (purple); the latter pore is predicted to have a conductance very close to limit 2, while the former will have a conductance closer (although not exactly equal) to limit 1.

(see figure 2(a)). We can approximate such a pore surface by the hyperboloid

$$x^2 + y^2 = z^2 \frac{D^2 - d^2}{l^2} + \frac{d^2}{4}, \tag{4}$$

in which $x^2 + y^2 = (d/2)^2$ at $z = 0$ and $x^2 + y^2 = (D/2)^2$ at $z = \pm l/2$. For this hourglass-shaped pore, we can find an exact solution for the resistance R_{hyp} between the two blue equipotential pieces of a spheroid depicted in figure 2(a). To do so, we solve analytically, by standard methods, the Laplace equation with proper boundary conditions, as given by the pore shape (see SI for details, available at stacks.iop.org/Nano/22/315101/mmedia). This yields the following expression:

$$R_{\mathrm{hyp}} = \frac{2\rho}{\pi d} \frac{\sin\alpha}{1 - \cos\alpha} \arctan\left(\frac{\sqrt{D^2 - d^2}}{d}\right), \tag{5}$$

where α is the asymptotic opening angle of the hyperboloid (see figure 2(a)) given by

$$\sin^2\alpha = \frac{D^2 - d^2}{l^2 + D^2 - d^2}. \tag{6}$$

Now, we have to include the access resistance from the pore to infinity. Unfortunately, it appears difficult to properly match the contributions from the access resistance and from the pore itself. However, we know the resistance from infinity to the purple hemisphere in the inset of figure 2(b) (given by $\rho/\pi D$ as determined by Hille [6, 7]), and the resistance from infinity to the orange disc (given by $\rho/2D$ from the calculation by Hall [8]). Since the blue cupola is always in between the purple and orange lines, we can state the following upper and lower limits on the total resistance:

$$R_{\mathrm{hyp}} + \frac{2\rho}{\pi D} < R < R_{\mathrm{hyp}} + \frac{\rho}{D}, \tag{7}$$

where R is the full measured resistance between remote electrodes.

From experimental studies of the pore shape [10–14], we deduce that $D \approx d + 20$ nm for typical beam conditions (note that the exact pore shape depends on the TEM beam conditions and hence might not be the same even for pores of equal diameter). Figure 2(b) shows the experimental data for $G(d)$ and compares them with the hyperboloid model calculations for the two limits of equation (7). Note that, upon adopting the experimental result for $D(d)$, the hourglass model has no adjustable parameters. The model predictions for the two bounds (two lines in figure 2(b)) bracket the data remarkably well. Note that the cylindrical model can only be forced to fit the data at the expense of adjusting the 'effective' membrane thickness to an incorrect value (in our case the best fit was for 8.6 nm, i.e., less than half the actual membrane thickness of 20 nm). In conclusion, we find that the hyperboloid model works better than the cylindrical model.

Having obtained an adequate description of the ionic conductance of solid-state nanopores we now ask: how does the conductance change upon insertion of a DNA molecule into the pore? Naively, one might expect the change in conductance upon insertion of a DNA molecule into the pore, ΔG, to be constant, independent of pore diameter, since the molecular volume that is blocking part of the pore is the same in all cases. However, we measured ΔG for B-form double stranded DNA (λ-DNA) for a number of pore sizes, and we find that ΔG clearly decreases with pore diameter. Typical events of DNA translocation through pores of diameters of 5, 15, and 65 nm are shown in figure 3(a). Experimental values for ΔG versus pore diameter are presented in figure 3(b).

The simple model of equation (1) fails to describe $\Delta G(d)$, as it would predict a constant ΔG. Instead, let us first consider the model of a cylindrical pore including the access resistance (equation (3)) and examine its prediction for the reduction in the conductance when DNA translocates through the pore. Although the DNA molecule is present both inside and outside the pore, its presence has a larger effect on the pore resistance than on the access resistance, because its volume fraction inside the pore (the volume of the DNA divided by the volume

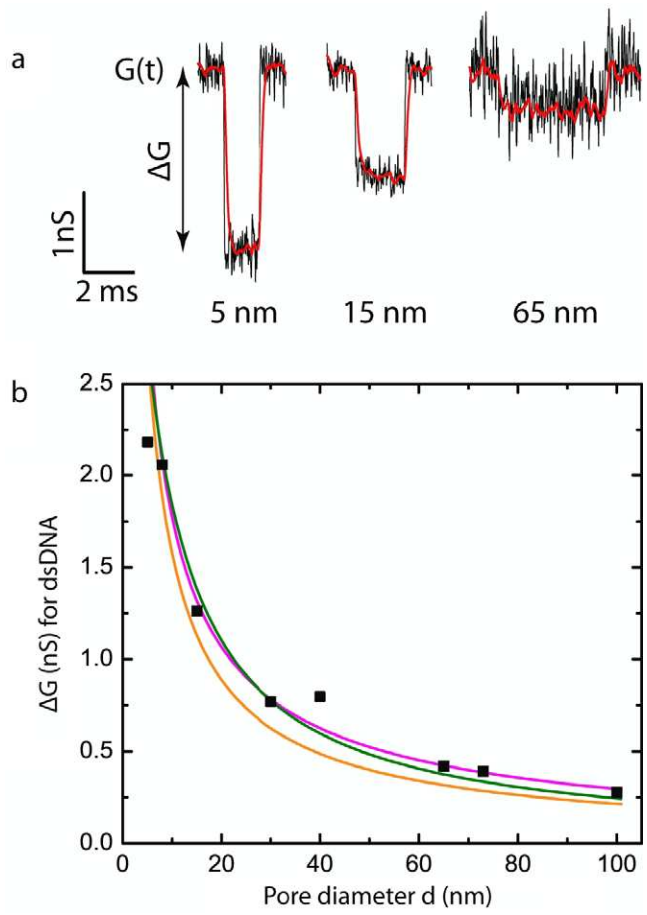

Figure 3. (a) Typical ionic conductance $G(t)$ traces when a DNA molecule translocates a nanopore of 5 nm (left), 15 nm (middle) or 65 nm (right) in diameter. The open pore conductance was 18 nS, 81 nS, and 599 nS, respectively. The data are low-pass filtered at 10 kHz (black) and 2 kHz (red). (b) Experimental data for the change in pore conductance ΔG upon insertion of a dsDNA molecule, as a function of pore diameter. The solid lines are for a simple geometric model with cylindrical DNA in a cylindrical pore (green), and in a hyperboloid-shaped pore in two limits (purple and orange; same color coding as in figure 2(b)).

inside the pore) is much larger than that outside the pore. For large pores, where the access resistance dominates the total resistance, the presence of DNA in the pore thus has a relatively smaller effect and ΔG decreases compared to its value for narrow pores. Based on geometrical considerations, we can calculate ΔG simply as

$$\Delta G = G_{\text{open pore}} - G_{\text{with DNA}} = G(d) - G(d_{\text{with DNA}}), \quad (8)$$

where G is given by equation (3) and $d_{\text{with DNA}}$ is the effective diameter of the pore with DNA in the pore, given by

$$d_{\text{with DNA}} = \sqrt{d^2 - d_{\text{DNA}}^2}. \quad (9)$$

Taking $d_{\text{DNA}} = 2.2$ nm, for B-form double stranded DNA, this simple model fits the data for ΔG for dsDNA versus pore diameter d remarkably well without any free fit parameters (blue line in figure 3(b); $\chi^2_{\text{red}} = 1.97$). Here we adopted the effective membrane thickness $l = 8.6$ nm, as found from fitting the data in figure 1. A least-squares fit with l as a free parameter gives a similar value, $l = 11.0$ nm, with almost the same χ^2_{red} value of 1.92.

Note that the case of single stranded DNA is more complex, and will not be considered in this paper, because single stranded DNA is very flexible, and therefore will coil up in a complex way in the access resistance region, contributing in an unpredictable way to ΔG. Furthermore, it was experimentally found that ΔG for ssDNA depends on the DNA sequence: while ssDNA homopolymers produce relatively small conductance blockade amplitudes [17], heteropolymeric ssDNA produces very large amplitudes [18]. Including these factors goes beyond our current modeling, which is only valid for polymers with a persistence length (∼1 nm for ssDNA; ∼50 nm for dsDNA) that is longer than the pore length (20 nm in our case).

Alternatively, one may use the same approach (i.e., equations (8) and (9)) to calculate ΔG when the (cylindrical) DNA is inside an hourglass-shaped pore with $l = 20$ nm (i.e., with G as given by equation (7)). This yields similar results, with $\chi^2_{\text{red}} = 1.63$ for limit 1 and $\chi^2_{\text{red}} = 6.3$ for limit 2 (see figure 3(b)). A different model was used by Wanunu *et al* [19]; however, they extracted the open pore conductance from measurements (rather than from a model), and only considered a limited size range of very narrow pores (2.7–4.7 nm in diameter). Finally, in SI section 4 (available at stacks.iop.org/Nano/22/315101/mmedia), we present a model for ΔG with dsDNA in the pore for which the solution in the closed form is obtained, where the DNA molecule is treated as a hyperboloid inserted along the symmetry axis of the hourglass-shaped pore. Note that, while DNA is obviously better modeled as a cylinder, the assumption that both the DNA and the pore have the same hyperbolic geometry simplifies the boundary conditions and allows an analytical solution of the Laplace equation for the electrostatic potential in the pore. We find that this model fits the experimental data reasonably well (figure S8 available at stacks.iop.org/Nano/22/315101/mmedia). While having academic value, this model is less practical in usage since DNA obviously is not a hyperboloid.

In conclusion, we have presented new experimental data on nanopore conductance and DNA blockade for a large range of pore sizes. We have developed several theoretical models to describe both, and obtained excellent agreement between theory and experiments. We have found that, in general, it is essential to include both the access and the pore resistance. An exact solution for the open pore conductance G of an hourglass-shaped pore agrees, without any adjustable parameters, with measurements of G. Additionally, we measured the conductance blockade ΔG due to the insertion of a dsDNA molecule for a number of pore sizes, and we found that ΔG strongly decreases with pore diameter, contrary to the predictions of earlier models that forecasted a constant ΔG. We developed several models for ΔG that provide excellent agreement with our experimental data. The models for G and ΔG presented in this paper can provide the foundation for understanding a multitude of conductance-based experiments on nanopores.

1. Materials and methods

1.1. Solid-state nanopores

Fabrication of solid-state nanopores starts with the fabrication of 20 nm thin free-standing SiN membranes through the use of electron-beam lithography and wet etching [20]. For the electrical measurements, a membrane with a single nanopore is mounted in a polyether ether ketone (PEEK) microfluidic flow cell and sealed to liquid compartments on either side of the sample. Measurements are performed in 1 M KCl salt solution containing 10 mM Tris-HCl and 1 mM EDTA at pH 8.0 at room temperature. Ag/AgCl electrodes are used to detect ionic currents and to apply electric fields. Current traces are measured at 10 kHz bandwidth using a resistive feedback amplifier (Axopatch 200B, Axon Instruments) and digitized at 100 kHz. For the dsDNA unmethylated λ-DNA (10 ng μl^{-1}, Promega, Madison, WI) was used. The event-fitting algorithm used to analyze and label the translocation events was the same as the one described before [21].

1.2. Fitting

The lowest reduced χ^2_{red} value was calculated using $\chi^2_{\mathrm{red}} = \frac{1}{N-n-1}\sum_{i=1}^{N}(\frac{X_i-\mu_i}{\sigma_i})^2$, with N the number of data points and n the number of fitting parameters. The error of the experimental data points is estimated at $\sigma_i = 0.1 \times G$, a relative error of 10%. Fitting was carried out using a custom written code in Matlab (see SI, section 7, available at stacks.iop.org/Nano/22/315101/mmedia).

Acknowledgments

We acknowledge discussions with G F Schneider. This work is supported by the NanoSci-E+ program, the European Union's Seventh Framework Programme (FP7/2007-2013) under grant agreement no. 201418 (READNA), and ERC-2009-AdG Grant 247072 NANOFORBIO. YR and AYG would like to acknowledge the support of the US–Israel Binational Science Foundation. YR would like to thank the Israel Science Foundation for financial support.

References

[1] Dekker C 2007 Solid-state nanopores *Nat. Nanotechnol.* **2** 209–15
[2] Branton D *et al* 2008 The potential and challenges of nanopore sequencing *Nat. Biotechnol.* **26** 1146–53
[3] Smeets R M M *et al* 2006 Salt dependence of ion transport and DNA translocation through solid-state nanopores *Nano Lett.* **6** 89–95
[4] Wanunu M, Morrison W, Rabin Y, Grosberg A Y and Meller A 2009 Electrostatic focusing of unlabeled DNA into nanoscale pores using a salt gradient *Nat. Nanotechnol.* **5** 160–5
[5] Grosberg A Y and Rabin Y 2010 DNA capture into a nanopore: interplay of diffusion and electrohydrodynamics *J. Chem. Phys.* **133** 165102
[6] Hille B 1968 Pharmacological modifications of the sodium channel of frog nerve *J. Gen. Physiol.* **51** 199–219
[7] Hille B 1970 Ionic channels in nerve membranes *Progress in Biophysics and Molecular Biology* vol 21, ed J A V Butler (New York: Pergamon) p 1
[8] Hall J E 1975 Access resistance of a small circular pore *J. Gen. Physiol.* **66** 531–2
[9] Vodyanoy I and Bezrukov S M 1992 Sizing of ion pore by access resistance measurements *Biophys. J.* **62** 10–1
[10] Liebes Y *et al* 2010 Reconstructing solid state nanopore shape from electrical measurements *Appl. Phys. Lett.* **97** 223105
[11] Kim M J, McNally B, Murata K and Meller A 2007 Characteristics of solid-state nanometre pores fabricated using a transmission electron microscope *Nanotechnology* **18** 205302
[12] van den Hout M *et al* 2010 Controlling nanopore size, shape and stability *Nanotechnology* **21** 115304
[13] Kim M J, Wanunu M, Bell D C and Meller A 2006 Rapid fabrication of uniformly sized nanopores and nanopore arrays for parallel DNA analysis *Adv. Mater.* **18** 3149–53
[14] Wu M-Y *et al* 2009 Control of shape and material composition of solid-state nanopores *Nano Lett.* **9** 479–84
[15] Haynes W M (ed) 2010 *CRC Handbook of Chemistry and Physics* 91st edn (Boca Raton, FL: CRC Press)
[16] Purcell E M 1984 *Electricity and Magnetism* (*Berkeley Physics Course* vol 2) (New york: McGraw-Hill) chapter 4 (Problem 4.10)
[17] Skinner G M *et al* 2009 Distinguishing single- and double-stranded nucleic acid molecules using solid-state nanopores *Nano Lett.* **9** 2953–60
[18] Kowalczyk S W *et al* 2010 Unraveling single-stranded DNA in a solid-state nanopore *Nano Lett.* **10** 1414–20
[19] Wanunu M, Sutin J, McNally B, Chow A and Meller A 2008 DNA translocation governed by interactions with solid-state nanopores *Biophys. J.* **95** 4716–25
[20] Kowalczyk S W, Hall A R and Dekker C 2010 Detection of local protein structures along DNA using solid-state nanopores *Nano Lett.* **10** 324–8
[21] Storm A J *et al* 2005 Fast DNA translocation through a solid-state nanopore *Nano Lett.* **5** 1193–7